TECHNICAL PAPER

A simple and efficient GIS tool for volume calculations of submarine landslides

David Julius Völker

Abstract A numeric tool is presented for calculating volumes of topographic voids such as slump scars of landslides, canyons or craters (negative/concave morphology), or alternatively, bumps and hills (positive/convex morphology) by means of digital elevation models embedded within a geographical information system (GIS). In this study, it has been used to calculate landslide volumes. The basic idea is that a (singular) event (landslide, meteorite impact, volcanic eruption) has disturbed an intact surface such that it is still possible to distinguish between the former (undisturbed) landscape and the disturbance (crater, slide scar, debris avalanche). In such cases, it is possible to reconstruct the paleo-surface and to calculate the volume difference between both surfaces, thereby approximating the volume gain or loss caused by the event. I tested the approach using synthetically generated land surfaces that were created on the basis of Shuttle Radar Topography Mission data. Also, I show the application to two real cases, (1) the calculation of the volume of the Masaya Slide, a submarine landslide on the Pacific continental slope of Nicaragua, and (2) the calculation of the void of a segment of the Fish River Canyon, Namibia. The tool is provided as a script file for the free GIS GRASS. It performs with little effort, and offers a range of interpolation parameters.

Testing with different sets of interpolation parameters results in a small range of uncertainty. This tool should prove useful in surface studies not exclusively on earth.

Introduction

In marine geohazard studies, it is often desirable to estimate the volumes of rocks or sediments that have been displaced by mass wasting processes. Such data are particularly important as input parameters for numerical models serving to calculate the tsunamogenic potential of past mass wasting events (e.g., Watts et al. 2005). Depending on the type of mass wasting process, characteristic morphological features are created that in some way reflect the size of the rock mass involved. Typically, at the head of the mass wasting structure, the excavation of material leaves a depression that is bounded by headwalls, whereas the dislocated material is deposited downslope of the excavation site. The dumped material can represent either the whole initially removed mass (in the case of cohesive material), a part thereof (if a fraction of the slide is removed via turbidity currents, and distributed over larger areas), or even a larger volume, if additional material is entrained in the course of the transport from source to sink. The deposited material can have a number of shapes, some of which can be easily identified as being associated with mass wasting (e.g., dislocated slump blocks and debris lobes; e.g., Hampton et al. 1996; Hühnerbach and Masson 2004). The distance between the excavation site and the deposition site can be anything from so short that both areas overlap, to some hundreds of kilometers.

The volume of the material involved can be estimated from both the negative (excavation, depression) and the

D. J. Völker (✉)
Leibniz Institute of Marine Sciences,
Christian-Albrechts Universität zu Kiel (IFM-GEOMAR),
Wischhofstr. 1-3,
24148 Kiel, Germany
e-mail: dvoelker@ifm-geomar.de

positive morphology (slump mass), if certain criteria are satisfied. The main criterion is that the paleo-surface be still well preserved in the vicinity of the bathymetrical feature of interest. In other words, the adjacent bathymetry would be very similar to that existing prior to the event that gave rise to the disturbance. Moreover, this background morphology needs to be geometrically simple (e.g., a slump block resting on an abyssal plain, or a spoon-shaped depression in a smooth continental slope). Ideally, in the case of mass wasting processes, there should be no overlap between the evacuation site and the deposition site, so that both volumes can be easily distinguished and calculated separately.

Swath bathymetric datasets of the seafloor are becoming ever more available at increasing resolution and precision. With growing coverage of submarine slopes of continental margins and islands of the world, there has been enhanced recognition of the importance of downslope transport processes in shaping the seafloor. Indeed, the number of detected and described submarine slides is increasing continuously, as is our notion of their variability in size, shape, and internal deformation (e.g., Masson et al. 2006). Compared to these advances, however, our understanding of triggering processes and boundary conditions lags behind. In order to establish relations between climate, sedimentation, seismicity, and the size and spatial frequency of landslides, a simple and effective tool, able to calculate the volumes of submarine landslides, is evidently needed. Such a tool is presented here, together with some examples of application, and an evaluation of its performance (error margin).

The estimation of the rock volumes involved in land surface changes using digital elevation models derived from remote sensing is not new. For events that happen at present on land, one might directly compare the land surface form prior to and after, or even during the disturbing process, with high precision and resolution (e.g., Kerle 2002; Tsutsui et al. 2007; Roering et al. 2009). For seafloor processes of the past, we are generally working with data of much lower resolution, and we are faced with the problem of having to remodel the surface prior to the event (Canals et al. 2004). In the majority of studies of mass wasting at submarine slopes, the landslide scar volumes or the corresponding deposited volumes are estimated by mapping the surface area and assuming a mean thickness from seismic cross sections (e.g., McAdoo et al. 2000; Tappin et al. 2001; Imbo et al. 2003). In some studies, the surface is restored by manually selecting and editing grid points of a digital elevation model (DEM), which is a tiresome task for a grid of some hundred to some thousand data points. Also, once created, the resulting restored grids are unique masterpieces. The task can be partly automated by extending bathymetric contour lines from either side of the depression/elevated area across it, and interpolation in

between (e.g., Urgeles et al. 1999; Lamarche et al. 2008), or by removing the scar area from the grid and triangulation across the blank area (e.g., Vanneste et al. 2006). The main benefit of "the healer" GIS (geographical information system) tool lies in its ease of use, which enables one to quickly calculate a number of models that could make sense and thereby obtain a better idea of the possible ranges of rock volume related to the event.

Some limitations of the method for landslide volume estimation should be mentioned. First, the method accounts only for changes of surfaces. In the case of buried slide bodies, three-dimensional seismic data are necessary to resolve the geometry (e.g., Gee et al. 2006; Winkelmann et al. 2006). Second, the method resolves the bulk volume of mass wasting deposits, i.e., the amount of displaced material today. This volume may differ from the rock volume removed, as the transport process produces an increase in the material porosity (Lamarche et al. 2008). This difference is related to the specific mass wasting process and the transported material involved in a given event.

Methodology

The tool described here, and named "the healer", is written for the open source Geographical Resources Analysis Support System (GRASS; Neteler and Mitasova 2004) to run on a UNIX/Linux platform. It makes use of standard UNIX commands such as awk and the bash-shell, as well as the basic calculator (bc), an arbitrary precision numeric processing language that is provided with most Linux distributions. It also uses commands of the Generic Mapping Tools (GMT; Wessel and Smith 1998). I choose this approach because GRASS is a very powerful and flexible GIS platform, GMT is very popular among geophysicists, both can be combined with UNIX and bc commands in shell scripts, and all of the software is freely available open source code. Most steps are done in a graphical user interface (GUI), with some dialogs.

Basically, the script creates new elevation values for a disturbed area, and performs an interpolation of these new data points and the points of the undisturbed area, using regularized spline with tension (Mitasova and Hofierka 1993). The following steps are executed:

1. The outline of the feature of interest is digitized as a closed polygon. This polygon is used to mask the original grid, and to export elevation values from outside of the mask.
2. A small number of so-called reference profiles are created outside of, but close to the masked area by clicking their endpoints. They represent the undisturbed

morphology, and serve as prototypes for calculating new data points to fill the masked area. Reference profiles should be straight lines that run either perpendicular or parallel to the slope.

3. A number of so-called patch profiles are created that span across the masked area. The endpoints have to lie outside of the masked area, but close to it. Each patch profile is related to a reference profile, and should follow roughly the same direction as that of the corresponding reference profile. Typically, for each reference profile about 20 or more patch profiles are produced.

4. The script calculates new z values for the x,y positions along the patch profiles, using the endpoint elevation values of the patch profiles and the morphology of the reference profiles. Thus, the masked area is being filled assuming that the seafloor once looked similar to the area covered by the reference profiles. The procedure is demonstrated in Fig. 1.

5. A new grid of the "restored" surface is created by interpolation of both the data points outside the masked area, and the newly created data points that are binned beforehand.

6. The differential volume between the original surface and the restored surface is calculated. It serves as an estimate of the volume gain or loss due to the event causing the disturbance.

The script provides an immediate graphical control of the restored surface. Normally, some iterations of step 3 are performed whereby more patch profiles are added to the data stack for interpolation in order to "stitch" enough data points across the blank area, until a satisfactory morphology is reached. Two parameters have a significant influence on the results of the interpolation, these being the bin size of the blockmean filter, B, and the tension parameter of the interpolation, T. Binning is performed to preprocess the newly created data points before interpolation. In this process, all data points within a certain rectangular area (the bin) are averaged to create a single value, which speeds up interpolation and also acts as a smoothing filter. Grid cell size I of the original grid and bin size B are expressed as edge length of a square cell, and B should be a simple multiple of I. The tension parameter determines the character of the resulting surface, from thin plate (stiff) to membrane (soft).

Results

In order to demonstrate the workflow, as well as to evaluate errors and interpolation parameters, three examples are presented below.

Example 1

Example 1 is a synthetic land surface, represented by a digital elevation model of 1 by 1° size (resolution of 556× 556 m per pixel). It is based on a land surface of South America extracted from the Shuttle Radar Topography Mission dataset (SRTM; Farr et al. 2007), cleaned for
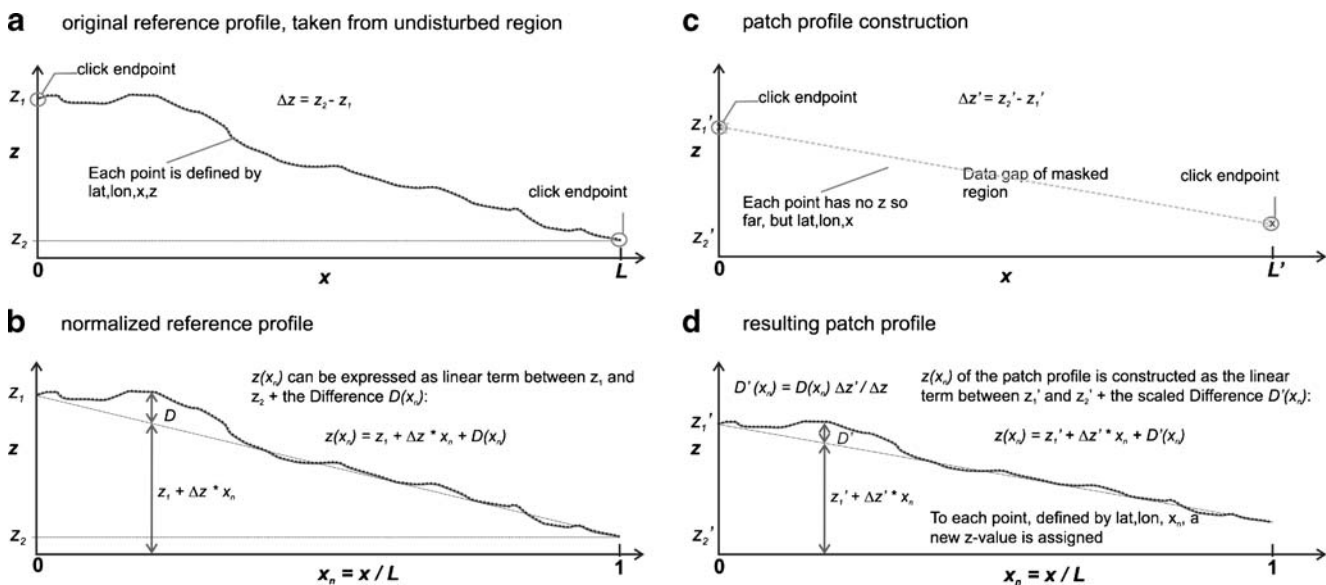

Fig. 1 Basic method of the creation of new elevation values along profiles crossing the masked area (patch profiles). **a** Reference profile, extracted from the area outside the masked area. **b** The profile is normalized to its length, and the sea surface elevation is expressed as a linear term plus deviation $D(x_n)$. **c** A patch profile is stretched across the masked area. **d** Elevation values are attributed to the coordinates of the individual points of the patch profile using a linear term between its endpoints plus the scaled deviation $D'(x_n)$

erroneous pixels, re-gridded, and superimposed with a simple box-shaped depression of defined volume. The depression lies on the slope of a flat-topped mountain with slope gradients <1°. The slope is partly incised by small gullies. Using the script, it is possible to restore the surface, and to calculate the volume of the depression serving as disturbance. The performance of the method and the chosen interpolation parameters can be evaluated by repeated trials

Fig. 2 Example 1: demonstration of the capability of the method to restore a surface using a modified landscape superimposed with a box-shaped depression of defined area and volume: **a** original 1×1° grid of the surface and central depression; **b**–**d** surfaces restored with a different number of patch profiles and changing interpolation parameters. The deviation from the known "missing" volume decreases with increasing number of patch profiles. Elevation ranges from 478 to 1,400 m, contour line interval is 100 m
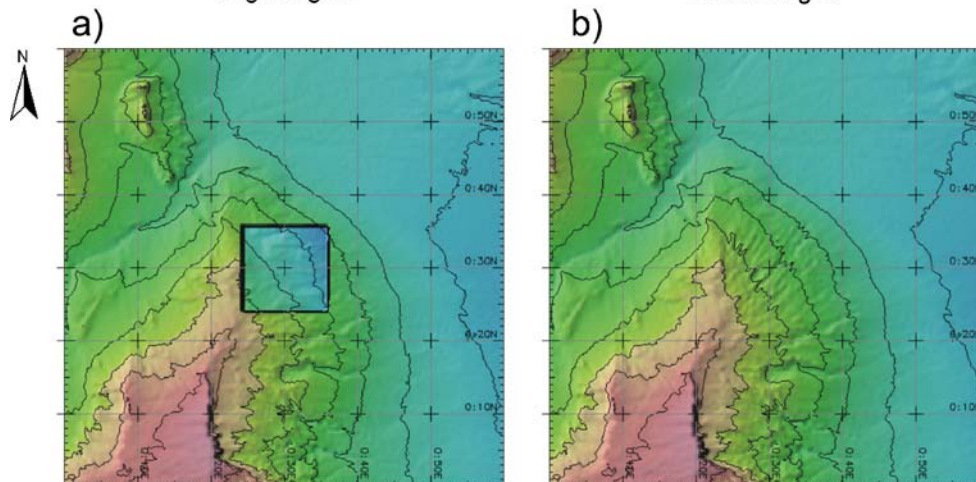

Example 01 - land topography overlain by an artificial distortion

SRTM data of 33-34°S, 69-70°W (Argentina)
Distortion: box-shaped depression
original grid

Grid cell size *I* : 0.005x0.005°
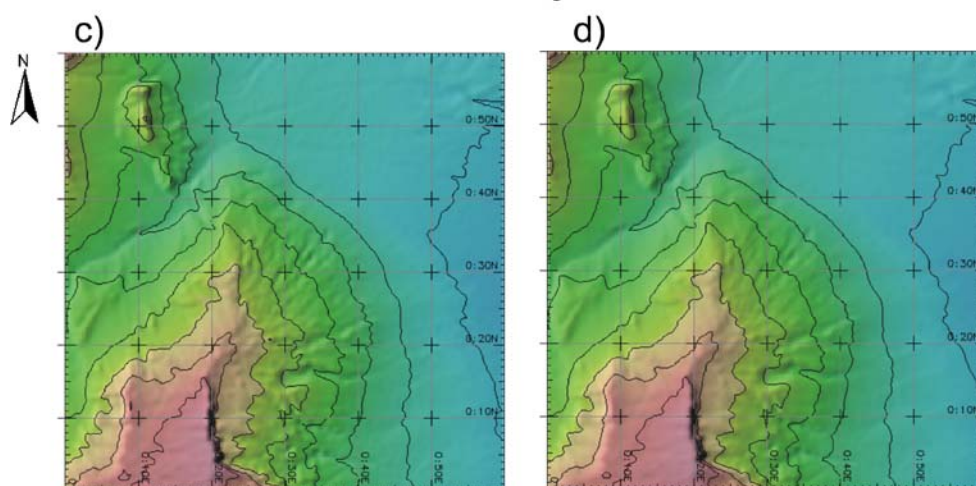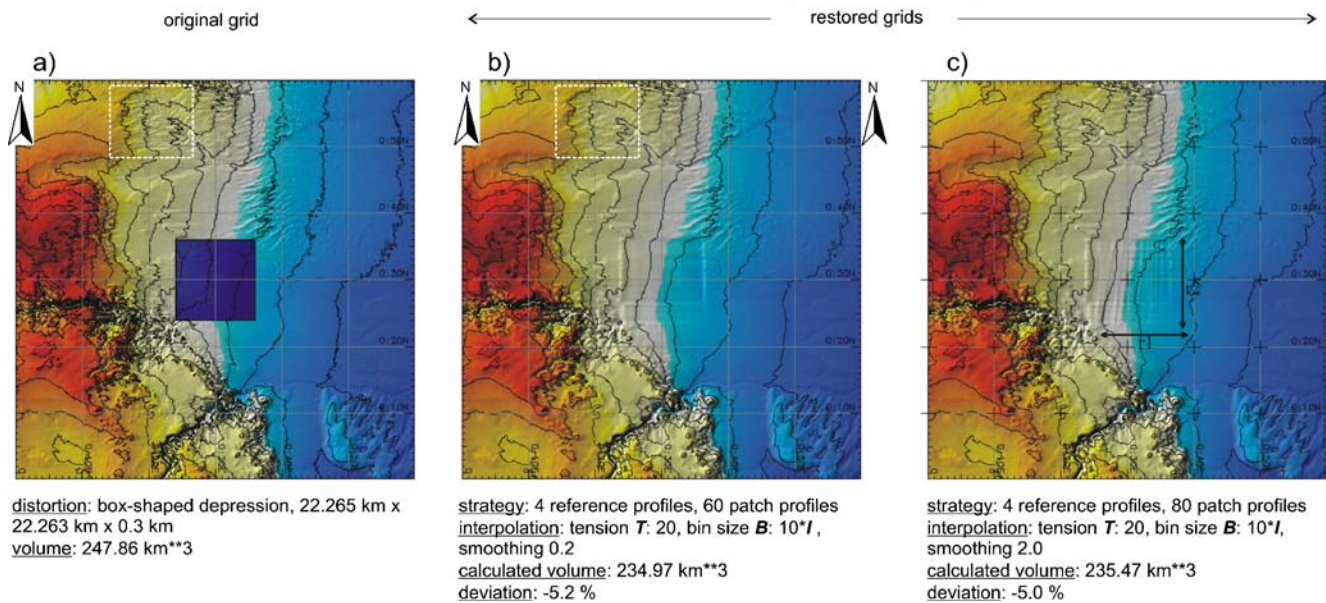Grid dimension: 200x200 cells
restored grid

a)

b)

distortion: box-shaped depression,
22.265 km x 22.263 km x 0.3 km
volume: 148.71 km**3

strategy: 4 reference profiles, 40 patch profiles
interpolation: tension *T*: 40,
bin size *B*: 1*I*, smoothing 0.1
calculated volume: 134.88 km**3
deviation: -9.3 %

restored grids

c)

d)

strategy: 4 reference profiles, 80 patch profiles
interpolation: tension *T*: 40, bin size *B*: 2*I*, smoothing 2.0
calculated volume: 138.96 km**3
deviation: -6.6 %

strategy: 4 reference profiles, 80 patch profiles
interpolation: tension *T*: 40, bin size *B*:2*I*, smoothing 5.0
calculated volume: 142.01 km**3
deviation: -4.5 %

original grid ← restored grids →

a)

b)

c)

distortion: box-shaped depression, 22.265 km × 22.263 km × 0.3 km
volume: 247.86 km**3

strategy: 4 reference profiles, 60 patch profiles
interpolation: tension *T*: 20, bin size *B*: 10*l, smoothing 0.2
calculated volume: 234.97 km**3
deviation: -5.2 %

strategy: 4 reference profiles, 80 patch profiles
interpolation: tension *T*: 20, bin size *B*: 10*l, smoothing 2.0
calculated volume: 235.47 km**3
deviation: -5.0 %

Fig. 3 Example 2: operation on another synthetic landscape superimposed with a *box-shaped* depression: **b** shows the result after using 60 patch profiles; note that a "ghost" of the *box shape* remains; **c** shows the effect of patch profile accumulation; compared to **b**, 20 patch profiles were added as a "cross stitch". Elevation ranges from 250 to 1,900 m, contour line interval is 100 m. The *stippled box* indicates a region where blurring of the grid produced by "the healer" in relation to the original grid (**a**) is notable. *Arrows* in **c** indicate position of the two reference profiles. Each reference profile coined 40 patch profiles to "stitch across" the depression

(Fig. 2). The difference between known and calculated volume gives a rough estimate of the range of uncertainty.

For example 1, 40 patch profiles are sufficient to restore a surface that is sufficiently similar to the adjacent slope. Using more patch profiles, and gridding parameters that tend to smoothen the surface, improves the result in terms of roughness of the surface and in terms of the volume deviation, from ca. −10 to ca. −4%.

If the bin size *B* exceeds 10 and/or the tension parameter *T* is lower than 10 ("stiff plate" character of resulting surface), differences between the morphology of the basic grid and the new grid outside of the masked area become observable, as the new grid becomes blurred. Minor blurring is observable in Fig. 3b (stippled box), where some details of erosional gullies observable in the original grid of Fig. 3a are lost.

Example 2

Like example 1, example 2 is a synthetic land surface extracted from the SRTM dataset and superimposed with a box-shaped depression. In this case, with the same dimensions the resolution is higher (222×222 m). The topography is steeper, with a gradient ranging between 0 and 3°, and more complex, with meandering gullies and floodplain morphology, thus increasing the difficulty of the task. Still, with 60 patch profiles, a satisfactory representation of a hypothetical paleo-surface was reached (Fig. 3b).

The calculated volume is close to the known volume (deviation of −5.2%). The outline of the box is still visible as a low-relief rim upslope, and a low-relief depression at the downslope end of the masked feature. This is due to the overlap of the patch profiles over the masked area.
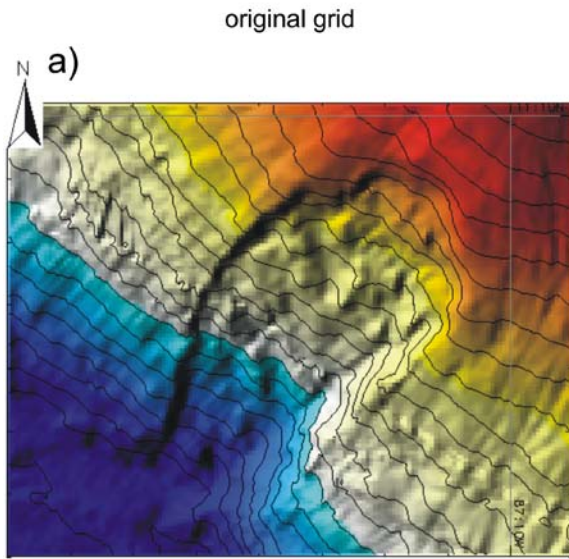
Example 3

The third example is the real case of a submarine landslide scar on the Pacific continental slope of Nicaragua, between 1,300 and 4,000 m water depth in a DEM of 14′×15′ and a resolution of 100×100 m (150×200 pixels; Fig. 4). This feature was observed during the Research Vessel *SONNE* cruises SO163 and SO173 with a SIMRAD EM120 swath bathymetry echosounder. It was termed the Masaya Slide, and has been described by Harders et al. (2006) and Talukder et al. (2008). I use this example to demonstrate the steps to perform with the described script. In this case, 140 patch profiles, created from five reference profiles, were necessary to produce a satisfactory model, fairly free of blocky and stripy interpolation effects. Surprisingly, the volume of the scar is more than double the estimate of 5.5 km³ reported by Harders et al. (2006). This value was calculated by multiplying the scarp area with a thickness derived from a sediment echosounder profile of the Parasound System. The mismatch might be due to the fact that the Parasound System performs poorly on slopes exceeding a gradient of some degrees.
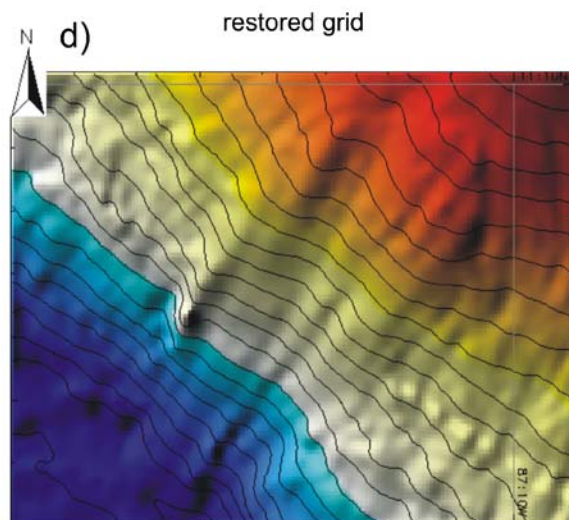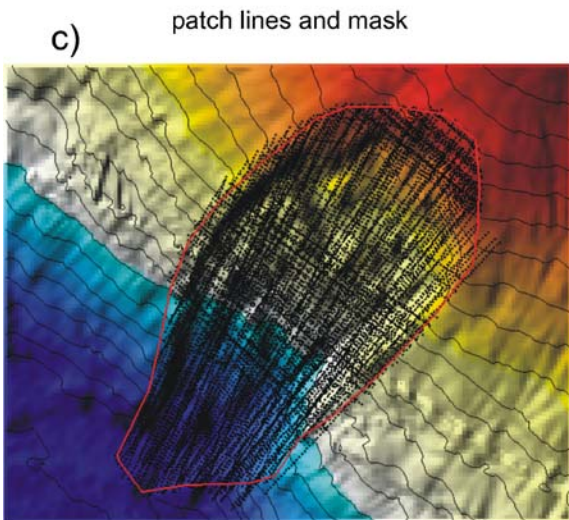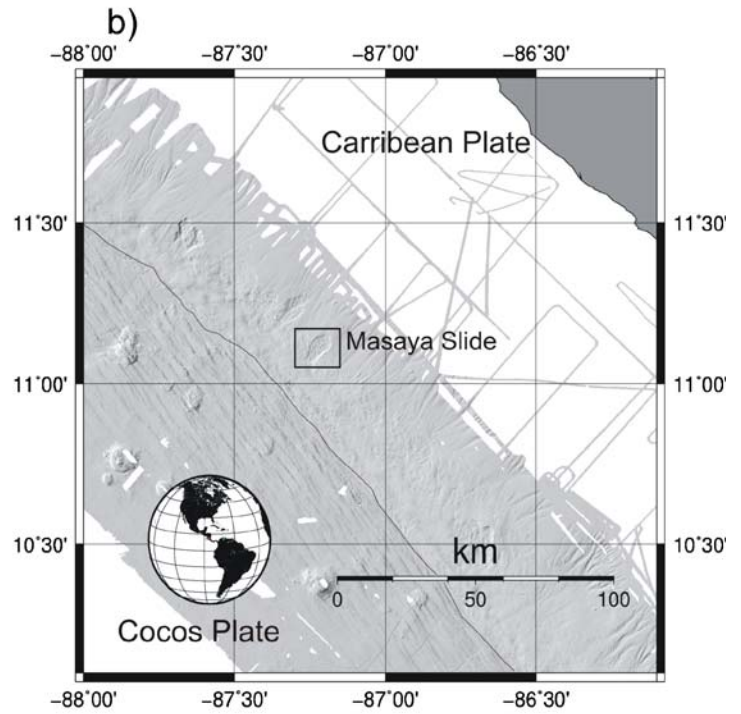
Example 03 - Masaya slide scar offshore
Nicaragua

Combined swath bathymetry data set of RV SONNE cruises
SO163 and SO173

Grid cell size *I*: 0.001 x 0.001°
Grid dimension: 150 x 120 Pixel

original grid

a)

distortion: 300 m deep spoon-shaped depression,
caused by submarine landslide

b)

Carribean Plate

Masaya Slide

Cocos Plate

patch lines and mask

c)

restored grid

d)

140 patch profiles
interpolation: tension *T*: 40, bin size *B*: 4**I*,
smoothing 0.2
calculated volume: 11.92 km**3

Fig. 4 Example 3: real case study of a submarine landslide scar offshore the Pacific coast of central Nicaragua (Masaya Slide): **c** demonstrates the data point creation procedure where the masked area outlined in *red* is patched by cross-stitching with patch profiles; **d** displays one of the possible results. The volume of the void is much higher than that estimated by Harders et al. (2006). Water depth ranges from 1,300 to 4,000 m, contour line interval is 100 m

Concluding remarks

The GRASS GIS tool described in, and provided with this article serves well to reconstitute disturbed paleo-surfaces with little effort. By variation of T and I, satisfactory results can be reached with a small number of patch profiles. The uncertainty can be estimated as the relative difference between the known volumes of the synthetic anomalies in examples 1 and 2, and the values calculated in a number of model runs with the tool. The degree of uncertainty depends on the areal extent and volume of the disturbance, and the complexity and steepness of the background area. The number of patch profiles needed to obtain satisfactory results depends on the general morphological complexity of the area, and the resolution of the basic grid. Also, the shape of the blank area, as well as its orientation in relation to the slope have some influence, as irregular shapes require more reference profiles than do shapes with straight boundaries that are aligned in line with or perpendicular to the slope.

It is stressed that the volumes calculated by means of "the healer" represent only those features that are visible from surface data. Depressions do become filled up by subsequent events, and sediment bodies eroded. This aspect has to be considered separately. The same applies to the fact that slumped blocks might become partly buried as they plough into soft sediments.

This simple and effective numeric tool to perform volume calculations of submarine mass wasting features in the open source GIS GRASS can be used in any other attempts to assess volume changes due to surface processes, provided that the paleo-surface is still well preserved adjacent to the disturbance, and that it is geometrically not too complex. Although not yet tested by the author, this tool should prove useful in surface studies not exclusively on earth.

The script and the sample datasets of shown examples, as well as a short, step-by-step guide (user manual) for the setup and use of the script are provided in the "Supplementary electronic material" of this article, available online to authorized users.

References

Canals M, Lastras G, Urgeles R, Casamor JL, Mienert J, Cattaneo A, De Batist M, Haflidason H, Imbo Y, Laberg JS, Locat J, Long D, Longva O, Masson DG, Sultan N, Trincardi F, Bryn P (2004) Slope failure dynamics and impacts from seafloor and shallow sub-seafloor geophysical data: case studies from the COSTA project. Mar Geol 213(1/4):9–72

Farr TG, Rosen PA, Caro E, Crippen R, Duren R, Hensley S, Kobrick M, Paller M, Rodriguez E, Roth L, Seal D, Shaffer S, Shimada J, Umland J, Werner M, Oskin M, Burbank D, Alsdorf D (2007) The shuttle radar topography mission. Rev Geophys 45:RG2004. doi:10.1029/2005RG000183

Gee MJR, Gawthorpe RL, Friedmann SJ (2006) Triggering and evolution of a giant submarine landslide offshore Angola, revealed by 3D seismic stratigraphy and geomorphology. J Sed Res 76:9–19

Hampton MA, Lee HJ, Locat J (1996) Submarine landslides. Rev Geophys 34:33–59

Harders R, Brückmann W, Feeser V, Hensen C, Kutterolf S (2006) Ash layers: the controlling factor on translational sliding offshore Central America? AGU Fall Meeting, 11–15 December 2006, San Francisco, CA, abstract #OS43C-0666

Hühnerbach V, Masson DG (2004) Landslides in the North Atlantic and its adjacent seas: an analysis of their morphology, setting and behaviour. Mar Geol 213(1/4):343–362

Imbo Y, Batist MD, Canals M, Prieto MJ, Baraza J (2003) The Gebra slide: a submarine slide on the Trinity Peninsula Margin, Antarctica. Mar Geol 193:235–252

Kerle N (2002) Volume estimation of the 1998 flank collapse at Casita volcano, Nicaragua: a comparison of photogrammetric and conventional techniques. Earth Surf Proc Land 27(7):759–772

Lamarche G, Joanne C, Collot J-Y (2008) Successive, large mass-transport deposits in the south Kermadec fore-arc basin, New Zealand: the Matakaoa submarine instability complex. Geochem Geophys Geosyst 9:Q04001. doi:10.1029/2007GC001843

Masson DG, Harbitz CB, Wynn RB, Pedersen G, Lovholt F (2006) Submarine landslides: processes, triggers and hazard prediction. Philos Trans R Soc A Math Phys Eng Sci 364(1845):2009–2039

McAdoo BG, Pratson LF, Orange DL (2000) Submarine landslide geomorphology, US continental slope. Mar Geol 169(1/2):103–136

Mitasova H, Hofierka J (1993) Interpolation by regularized spline with tension: II. Application to terrain modeling and surface geometry analysis. Math Geol 25:657–667

Neteler M, Mitasova H (2004) Open source GIS: a GRASS GIS approach. Kluwer International Series in Engineering and Computer Science (SECS), vol 689. Boston, Kluwer

Roering JJ, Stimely LL, Mackey BH, Schmidt DA (2009) Using DInSAR, airborne LiDAR, and archival air photos to quantify landsliding and sediment transport. Geophys Res Lett 36: L19402. doi:10.1029/2009GL040374

Talukder AR, Bialas J, Kläschen D, Brückmann W, Reston TJ, Petersen CJ (2008) Tectonic framework of the mud mounds, associated BSRs and submarine landslides offshore Nicaragua Pacific margin. J Geol Soc Lond 165:167–176

Tappin DR, Watts P, McMurtry GM, Lafoy Y, Matsumoto T (2001) The Sissano, Papua New Guinea tsunami of July 1998—offshore evidence on the source mechanism. Mar Geol 175(1/4):1–23

Tsutsui K, Rokugawa S, Nakagawa H, Miyazaki S, Cheng C-T, Shiraishi T, Yang S-D (2007) Detection and volume estimation of large-scale landslides based on elevation-change analysis using DEMs extracted from high-resolution satellite stereo imagery. IEEE Trans Geosci Remote Sens 45(6):1681–1696

Urgeles R, Masson DG, Canals M, Watts AB, LeBas T (1999) Recurrent large-scale landsliding on the west flank of La Palma, Canary Islands. J Geophys Res 104(B11):25,331–25,348

Vanneste M, Mienert J, Bünz S (2006) The Hinlopen slide: a giant, submarine slope failure on the northern Svalbard Margin, Arctic Ocean. Earth Planet Sci Lett 245(1/2):373–388

Watts P, Grilli ST, Tappin DR, Fryer GJ (2005) Tsunami generation by submarine mass failure. II. Predictive equations and case studies. J Waterway Port Coastal Ocean Eng 131(6):298–310

Wessel P, Smith WHF (1998) New, improved version of the generic mapping tools released. EOS Trans AGU 79:579

Winkelmann DW, Jokat W, Niessen F, Stein R, Winkler A (2006) Age and extent of the Yermak Slide north of Spitsbergen, Arctic Ocean. Geochem Geophys Geosyst 7:Q06007. doi:10.1029/2005GC001130